Remote Sensing of Environment 143 (2014) 64–72

Contents lists available at ScienceDirect

Remote Sensing of Environment

journal homepage: www.elsevier.com/locate/rse

Sensitivity of multi-parameter soil moisture retrievals to incidence angle configuration

Sandy Peischl [a], Jeffrey P. Walker [a,*], Nan Ye [a], Dongryeol Ryu [b], Yann Kerr [c]

[a] Department of Civil Engineering, Monash University, Australia
[b] Department of Infrastructure Engineering, The University of Melbourne, Australia
[c] Centre d'Etudes Spatiales de la Biosphère (CESBIO), Toulouse, France

ARTICLE INFO

Article history:
Received 20 June 2012
Received in revised form 20 November 2013
Accepted 23 November 2013
Available online xxxx

Keywords:
Multi-incidence angle
Passive microwave remote sensing
L-band
Soil moisture
Soil Moisture and Ocean Salinity (SMOS)

ABSTRACT

This paper focuses on the sensitivity of L-band multi-parameter retrievals across the range of angular measurements available from the SMOS (Soil Moisture and Ocean Salinity) mission. The SMOS core algorithm was used to evaluate two-parameter retrieval scenarios including soil moisture and one of either i) vegetation water content, ii) surface roughness, iii) vegetation temperature, or iv) surface soil temperature. For all pairs a range of parameter value combinations were compiled to run the model in forward mode. Subsequently, the resulting angular brightness temperature simulations with two unknown parameters were compared against the brightness temperature response derived from reference simulations using data from the National Airborne Field Experiment 2005 (NAFE'05) in Australia. This paper showed that the two-parameter retrieval accuracy of soil moisture is strongly affected by the surface moisture conditions, the polarization of the brightness temperature data, and the choice of the secondary ancillary parameter to be retrieved. The synthetic analysis demonstrated a tendency for better retrievals from dual-polarized data at large incidence angles (40–50°). Validation with airborne brightness temperature observations at L-band did not demonstrate such a strong angular dependency, although it confirmed that the simultaneous retrieval of soil moisture and vegetation properties is not preferable as opposed to i) soil moisture and surface roughness or ii) soil moisture and surface soil temperature, especially under dry moisture conditions.

1. Introduction

Passive microwave observations have been proven as one of the most promising techniques for near-surface soil moisture measurement (Jackson, 1993; Njoku & Entekhabi, 1996; Schmugge, O'Neill, & Wang, 1986; Walker & Houser, 2004; Wigneron et al., 2003). The high sensitivity to moisture and the robustness of the sensor signal in response to surface roughness and vegetation canopy effects make brightness temperature measurements in the protected microwave range of 1–2 GHz (L-band) the spectrum window of choice. A range of retrieval algorithms have been developed and tested using data collected from a series of small-scale truck and tower-based experiments, and airborne radiometers to a more limited extent (e.g. de Rosnay et al., 2006; Jackson et al., 1999; Saleh et al., 2004; Schmugge, Wang, & Asrar, 1988; Schmugge, Jackson, Kustas, & Wang, 1992; Wigneron, Calvet, Kerr, Chanzy, & Lopes, 1993; Wigneron, Kerr, Chanzy, & Jin, 1993; Wigneron, Schmugge, Chanzy, Calvet, & Kerr, 1998). These results ultimately contributed to the design of the first spaceborne instrument dedicated to global soil moisture mapping: the Soil Moisture and Ocean Salinity (SMOS) mission (Kerr, Font, Waldteufel, & Berger, 2000).

SMOS was launched by the European Space Agency (ESA) in November 2009 and operates in the 1.400–1.427 GHz L-band (McMullan et al., 2008). The satellite incorporates a novel interferometric synthesized antenna concept, utilizing over 69 small antenna patches distributed along the Y-shaped satellite arms and central hub (Kerr et al., 2010). This innovative satellite design yields multi-incidence angle brightness temperature observations ranging from 0° to 60° across a 900 km swath with an approximately 45 km spatial resolution and a 2–3 day recurrence interval at 6 A.M. and 6 P.M. local time. The sequence of snapshots obtained over the same pixel but at different incidence angles is intended to enhance the soil moisture retrieval to meet the target accuracy of 0.04 $m^3\ m^{-3}$, when the biomass density is lower than 4 $kg\ m^{-2}$ (Kerr et al., 2001).

The estimation of soil moisture from microwave observations becomes more complex with the presence of a vegetation layer above the surface compared to bare soil conditions. Although it is expected that at around 6 A.M. overpass time, conditions will be such that the vegetation and the soil surface will be close to thermal equilibrium, the additional interaction of the emitted energy with the vegetation canopy still needs to be accounted for. Consequently, a larger set of ancillary input parameters is required to accurately describe the ground

* Corresponding author.
E-mail addresses: spei2@student.monash.edu (S. Peischl), jeff.walker@monash.edu (J.P. Walker), dryu@unimelb.edu.au (D. Ryu), yann.kerr@cesbio.cnes.fr (Y. Kerr).

0034-4257/$ – see front matter © 2014 Elsevier Inc. All rights reserved.
http://dx.doi.org/10.1016/j.rse.2013.11.019

Table 1
Overview of the L-MEB input parameter values for the two experiment days.

Date	NAFE'05 ground measurements				Ancillary data					
	SM (std) [$m^3\ m^{-3}$]	VWC [$kg\ m^{-2}$]	T_{veg} [K]	T_{surf} [K]	H_R[a] [–]	N_R[b] [–]	b[a] [–]	ω[b] [–]	tt_H[b] [–]	tt_V[b] [–]
09.Nov	0.43 (±0.06)	1.9	309	303	0.8	0	0.08	0	1	8
23.Nov	0.14 (±0.05)	0.7	309	303						

[a] Sourced from Peischl et al. (2012).
[b] Sourced from Wigneron et al. (2007).

state. While much of these ancillary data can be obtained from i) point measurements at monitoring sites, ii) other spaceborne sensors, and iii) data assimilation models, there are issues with spatial and/or temporal discrepancies due to the variety of data sources. Therefore Wigneron, Waldteufel, Chanzy, Calvet, and Kerr (2000) considered the use of dual-polarized microwave data, acquired at multiple incidence angles by the same instrument, as an approach to overcome the need for ancillary data from external sources. They demonstrated the potential for simultaneous retrieval of soil moisture together with ancillary data, described as multi-parameter retrieval. Multi-angle observations also provide a possibility to reduce the impact of noise, such as radio frequency interference as experienced by SMOS (e.g. Camps et al., 2010; Castro, Gutierrez, & Barbosa, 2012; Oliva et al., 2012) by being able to identify RFI sources through angular anomalies.

If compared to the SMOS configuration only a very narrow range of angular observations is available, or if the SMOS angular range is reduced for some reason, then the benefits of multi-angle soil moisture retrievals might be compromised. In this context, it is necessary to assess the multi-parameter retrieval capability under alternate angular ranges and subsets of angles, to see if equivalent retrieval results can be achieved. Since the main parameters of interest beside soil moisture "SM" are: i) the vegetation water content "VWC" (through the vegetation optical depth), ii) the surface roughness conditions "H_R", iii) the surface soil temperature "T_{surf}", and iv) the vegetation temperature "T_{veg}" (in case of non-early morning brightness temperature measurements), these variables will be the focus of this study. Specifically, the questions addressed by this paper include:

1. What range of incidence angles for brightness temperature observations provides optimal multi-parameter results considering a maximum angular range for radiometric measurements of 0–50°?
2. Would a combination of brightness temperature observations from different angular groups yield better results compared to a specified range of incidence angles only?

A variety of land surface conditions are studied, including dry and wet soils under a mature wheat canopy with moderate and high vegetation water contents, to investigate these questions. This study differs from previous work on the sensitivity of multi-angle data measurements in so much that it includes a validation of findings from synthetic experiments using airborne L-band observations acquired at farm-scale resolution, while others have focused solely on ground-based observations (e.g. Calvet et al., 2011; Wigneron et al., 2000, 2004).

2. Radiative transfer model

The radiative transfer model used to simulate the wheat canopy emission at L-band, and to test the multi-parameter retrieval across varying ranges of incidence angles, is one of the core algorithms applied to SMOS data (Kerr et al., 2011, 2012). A detailed description of the L-band Microwave Emission for the Biosphere model (L-MEB) can be found in Wigneron et al. (2007), together with a parameter analysis for crop application and derived values for wheat canopy analysis. The inversion of the model allows the retrieval of soil moisture and ancillary data by minimizing the root mean square error between the simulated and reference brightness temperatures.

The interaction and individual contributions of the soil and vegetation media on the composite brightness temperature (TB) are accounted for in L-MEB using a radiative transfer approach, also called the tau-omega model (Mo, Choudhury, Schmugge, Wang, & Jackson, 1982):

$$TB_{(P,\theta)} = \left(1-\omega_{(P)}\right)\cdot\left(1-\gamma_{(P,\theta)}\right)\cdot\left(1+\gamma_{(P,\theta)}\cdot r_{G(P,\theta)}\right)\cdot T_C + \left(1-r_{G(P,\theta)}\right)\cdot\gamma_{(P,\theta)}\cdot T_G, \quad (1)$$

with P representing the measured polarization (H for horizontal, and V for vertical, respectively), θ the incidence angle, and T_G and T_C corresponding to the effective soil and vegetation temperature [K],

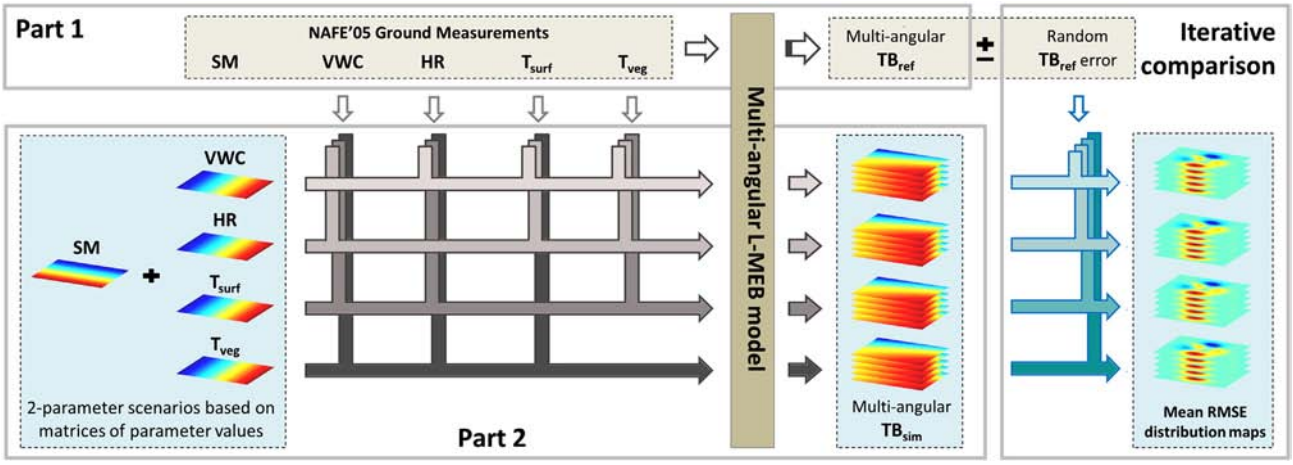

Fig. 1. Schematic of simulating synthetic multi-angular brightness temperature data (TB) using the forward model L-MEB. Part 1 illustrates the simulation of synthetic TB_{ref} based on NAFE'05 ground measurements. Part 2 describes the simulation of synthetic TB_{sim} based on NAFE'05 ground measurements and a matrix of two parameter value combinations depending on the scenario chosen (scenario: SM–VWC; SM–HR; SM–T_{surf}; or SM–T_{veg}). The final iterative comparison considers inclusion of a random TB error of maximum ±2 K for TB_{ref} and calculates the root mean square error between the varying TB_{ref} and TB_{sim} for each iteration step to arrive at a mean TB RMSE map.

Table 2
Range of values (min-max) tested in multi-parameter retrieval combinations.

SM [$m^3\ m^{-3}$]	VWC [$kg\ m^{-2}$]	H_R [−]	T_{veg} [K]	T_{surf} [K]
0–0.6	0–3	0–1.5	278–340	278–340

respectively. The reflectivity of non-smooth soil surfaces $r_{G(P,\theta)}$, which is sensitive to the incidence angle and the polarization, can be quantified using a modification of the Fresnel equation by including a set of soil roughness parameters H_R and $N_{R(P)}$:

$$r_{G(P,\theta)} = r^*_{G(P,\theta)} \cdot \exp\left[-H_R \cdot \cos\theta^{\left(N_{R(P)}\right)}\right]. \quad (2)$$

The Fresnel reflectivity $r^*_{G(P,\theta)}$ from a smooth, ideally flat surface can be related in turn to soil moisture content through a dielectric mixing model, such as the one developed by Dobson, Ulaby, Hallikainen, and El-Rayes (1985) that was used in this study. The model variables characterizing the canopy are the single scattering albedo $\omega_{(P)}$ and the vegetation transmissivity $\gamma_{(P,\theta)}$. The latter, also known as vegetation attenuation, is modeled as a function of the incidence angle and the optical depth at nadir τ_{NAD}:

$$\gamma_{(P,\theta)} = \exp\left[-\tau_{NAD} \cdot \left(\sin^2\theta \cdot tt_{(P)} + cos^2\theta\right) / \cos\theta\right] \quad (3)$$

with the vegetation structure parameters tt_H and tt_V correcting the optical depth for non-nadir viewing angles at each polarization. Hence, the optical depth increases with the amount of water on/in the canopy, which consequently reduces the transmission of the emitted soil energy within the vegetation medium. L-MEB assumes a linear relationship between the vegetation water content VWC and the nadir optical depth:

$$\tau_{NAD} = \mathrm{VWC} \cdot b_{(P)}, \quad (4)$$

where the empirical vegetation parameter $b_{(P)}$ is mainly dependent on the sensor frequency, polarization, canopy type and plant structure (Jackson & Schmugge, 1991).

3. Experimental dataset and model setup

The present study is based on both simulated brightness temperatures and radiometric measurements acquired over a wheat field during the November 2005 National Airborne Field Experiment (NAFE'05) in south-eastern Australia (Panciera et al., 2008). The campaign was conducted across selected focus farms in the Goulburn River catchment (31°46′S to 32°51′S and 149°40′E to 150°36′E), where a combination of airborne as well as extensive ground monitoring was carried out. The primary sensor operated aboard the aircraft was the Polarimetric L-band Multi-beam Radiometer (PLMR), which used six pushbroom receivers at along track incidence angles of nominally ±7°, ±21.5° and ±38.5°, respectively, for the flights analyzed in this study. The multi-angle observation mode was achieved by rotating the radiometer by 90°, and thus allowing three beams measuring forward and three beams backward along the flight direction. Due to an aircraft pitch of about 6°, the actual angles of the six PLMR beams were approximately 1°, 13°, 16°, 28°, 33°, and 45° along track. The radiometer was calibrated daily using cold/warm targets, with a calibration accuracy determined as being 0.7 K and 2 K for H- and V-polarization, respectively (Panciera et al., 2008). The multi-angle flights of this study were undertaken at an altitude of approximately 750 m (AGL), providing a spatial resolution of ~250 m.

Extensive ground monitoring was undertaken coincident with the airborne observations. High-resolution near-surface soil moisture measurements using the Hydraprobe Data Acquisition System (HDAS, Merlin et al., 2007) were taken across the focus farms (Panciera, Allahmoradi, Merlin, Young, & Walker, 2009). The Hydraprobe soil moisture sensor calibration was developed in the laboratory and from field samples, with a measurement accuracy of 0.04 $m^3\ m^{-3}$. The data used in this study were collected on four sampling days (once per week) within a cropping field of mature wheat canopy on silty clay loam soil, and capturing a dry down period within the observed time frame going from almost saturated soil surface (~0.43 $m^3\ m^{-3}$) to moderate-dry soil conditions (~0.14 $m^3\ m^{-3}$). The NAFE'05 in-situ soil moisture was averaged from ~250 HDAS measurements and the respective standard deviation calculated for use in the data analysis. The vegetation water content demonstrated a similar decrease from approximately 3 kg m^{-2} to 1 kg m^{-2}. Additional ground information about soil texture, surface roughness, soil profile temperature and soil

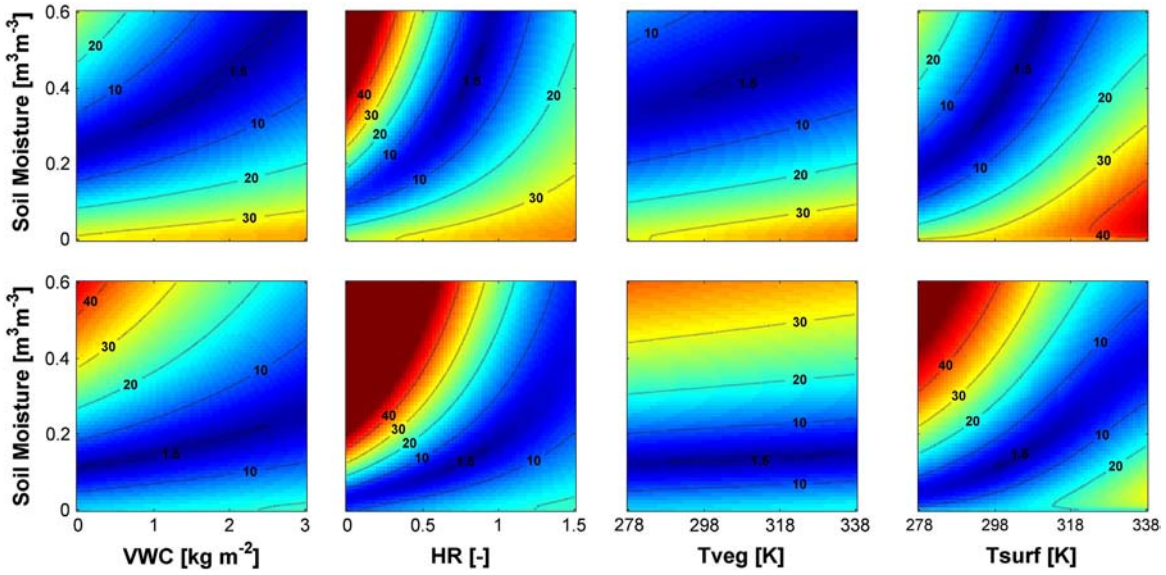

Fig. 2. Plots of mean TB RMSE distribution [K] for four scenarios of two-parameter combinations (SM–VWC, SM–HR, SM–T_{veg}, SM–T_{surf}). The RMSE was calculated from the iterative difference in TB_{ref} and TB_{sim} considering all dual-polarized TB data within 0–50° incidence angle range. The contour lines indicate the level of RMSE in the parameter space. The top row represents wet conditions (SM = 0.43 $m^3\ m^{-3}$, VWC = 1.9 kg m^{-2}) and the bottom row dry conditions (0.14 $m^3\ m^{-3}$, VWC = 0.7 kg m^{-2}).

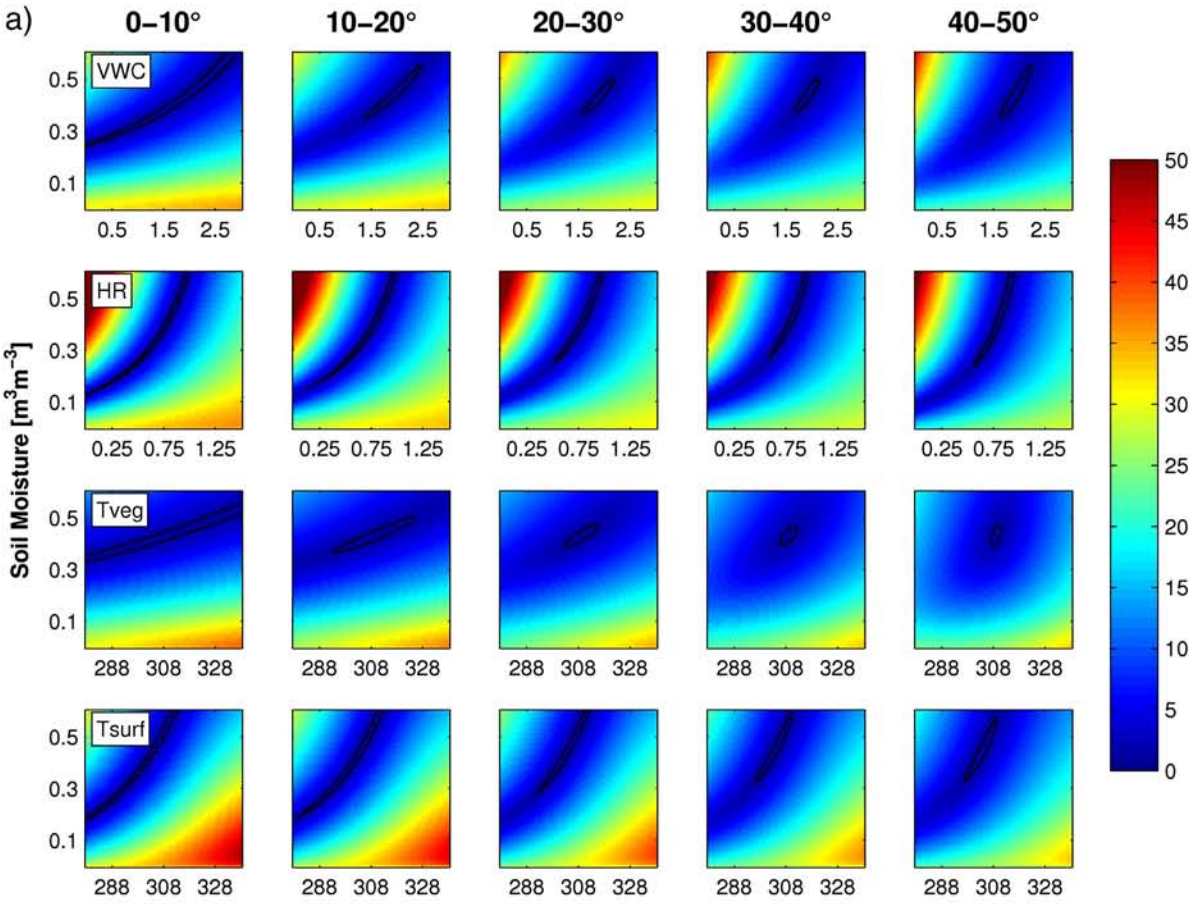
a)
0–10°
10–20°
20–30°
30–40°
40–50°
VWC
HR
Tveg
Tsurf
Soil Moisture [m³m⁻³]
0.5
0.3
0.1
0.5 1.5 2.5
0.25 0.75 1.25
288 308 328
50
45
40
35
30
25
20
15
10
5
0

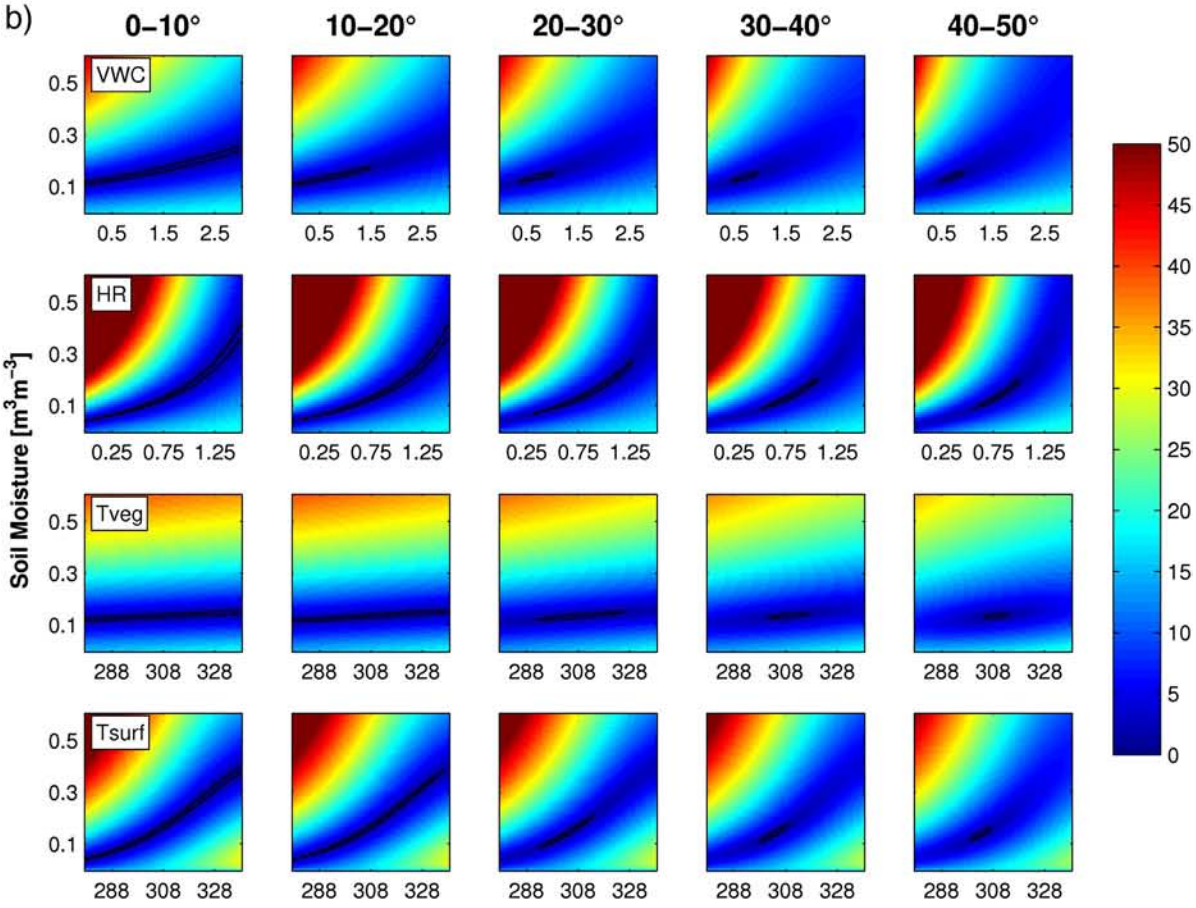
b)
0–10°
10–20°
20–30°
30–40°
40–50°
VWC
HR
Tveg
Tsurf
Soil Moisture [m³m⁻³]
0.5
0.3
0.1
0.5 1.5 2.5
0.25 0.75 1.25
288 308 328
50
45
40
35
30
25
20
15
10
5
0

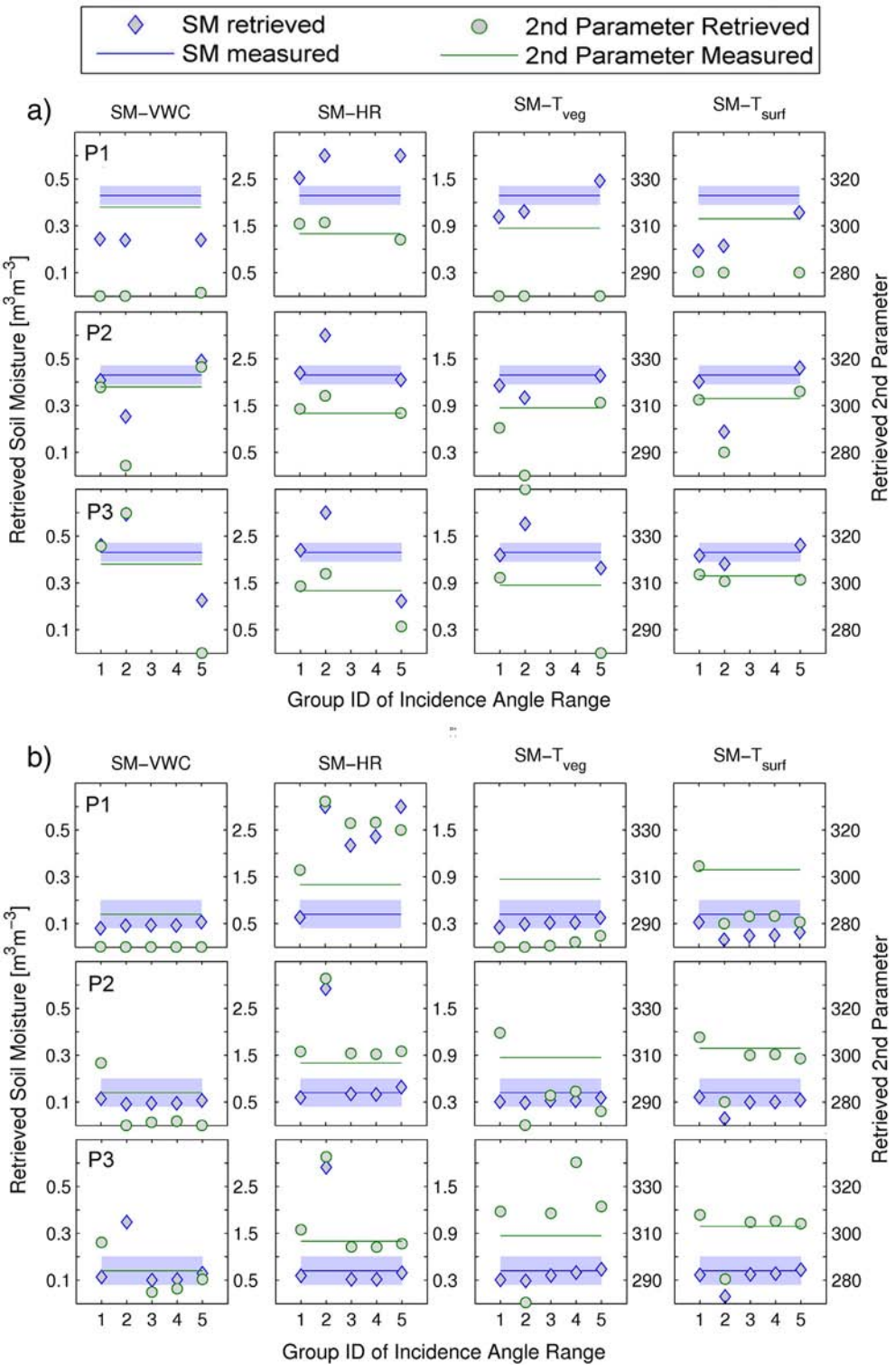

Fig. 4. Comparison of two-parameter retrieval results derived from the airborne dual-polarized NAFE'05 TB measurements, which were classified into five angular groups as shown on the x-axis (1: 0–10°; 2: 10–20°; 3: 20–30°; 4: 30–40°; 5: 40–50°). The shaded area depicts the standard deviation of the NAFE'05 ground measured soil moisture with the average value indicated by the blue line. Note that in each plot the left y-axis corresponds to the retrieved soil moisture and the right y-axis relates to the additionally retrieved parameter indicated at the top of each column: i) VWC [kg m^{-2}], ii) H_R [−], iii) T_{veg} [K], and iv) T_{surf} [K]. Panel (a) illustrates wet conditions with SM = 0.43 m^3m^{-3} and VWC = 1.9 kg m^{-2}, while panel (b) illustrates dry moisture conditions with SM = 0.14 m^3 m^{-3} and VWC = 0.7 kg m^{-2}, respectively. The index of each row relates to a different parameterization (P) used for the vegetation structure characterization in the retrieval model: i) P1: $tt_H = 1$, $tt_V = 8$; ii) P2: $tt_H = 0.2$, $tt_V = 1.4$; iii) P3: $tt_H = 1$, $tt_V = 1$. (For interpretation of the references to color in this figure legend, the reader is referred to the web version of this article.)

Fig. 3. Evolution of the mean dual-polarized TB RMSE distribution [K] across varying ranges of incidence angle for four scenarios of two-parameter combinations (rows 1 & 5: SM–VWC, rows 2 & 6: SM–HR, rows 3 & 7: SM–T_{veg}, rows 4 & 8: SM–T_{surf}). The black contour line indicates an RMSE level of 1.5 K. Panel (a) illustrates moist conditions with SM = 0.43 m^3 m^{-3}, VWC = 1.9 kg m^{-2}, and panel (b) illustrates dry conditions with SM = 0.14 m^3m^{-3} and VWC = 0.7 kg m^{-2}.

Table 3
Classification of angular groups according to incidence angle [°] and polarization (d — dual, h — horizontal, v — vertical).

ID	1	2	3	4	5	6
Angular range	0–50d (all)	0–10d	10–20d	20–30d	30–40d	40–50d

ID	7	8	9	10	11	12	13	14	15	16
Angular range	0–10d, 10–20d	0–10d, 20–30d	0–10d, 30–40d	0–10d, 40–50d	10–20d, 20–30d	10–20d, 30–40d	10–20d, 40–50d	20–30d, 30–40d	20–30d, 40–50d	30–40d, 40–50d
ID	17	18	19	20	21	22	23	24	25	26
Angular range	0–10h, 10–20v	0–10h, 20–30v	0–10h, 30–40v	0–10h, 40–50v	10–20h, 20–30v	10–20h, 30–40v	10–20h, 40–50v	20–30h, 30–40v	20–30h, 40–50v	30–40h, 40–50v
ID	27	28	29	30	31	32	33	34	35	36
Angular range	0–10v, 10–20h	0–10v, 20–30h	0–10v, 30–40h	0–10v, 40–50h	10–20v, 20–30h	10–20v, 30–40h	10–20v, 40–50h	20–30v, 30–40h	20–30v, 40–50h	30–40v, 40–50h

profile moisture were gathered from supplementary measurements made by the ground team and/or in-situ monitoring stations.

The synthetic analysis of this current study was based on simulated brightness temperature data that would represent the land surface conditions of the NAFE'05 test field using L-MEB. Table 1 presents an overview of the L-MEB parameter values used for the modeling. Processing of the synthetic brightness temperatures was divided into two parts, as indicated in Fig. 1. The first step focused on simulating a reference set of dual-polarized brightness temperatures (TB_{ref}) across incidence angles of 0–50° (top part in Fig. 1). This was achieved by feeding the forward model with all available NAFE'05 ground truth information and ancillary parameters (as given in Table 1). The resultant multi-angular TB_{ref} were subsequently perturbed, taking into account a random TB error of maximum ±2 K, corresponding to the V-polarization calibration error of the PLMR instrument.

The second step of data processing involved the simulation of multiple sets of microwave responses (TB_{sim}) by varying input data according to a range of two-parameter scenarios. The scenarios considered were: i) soil moisture and vegetation water content (SM–VWC), ii) soil moisture and surface roughness (SM–H_R), iii) soil moisture and vegetation temperature (SM–T_{veg}), or iv) soil moisture and surface soil temperature (SM–T_{surf}). For instance, according to the SM–VWC scenario it

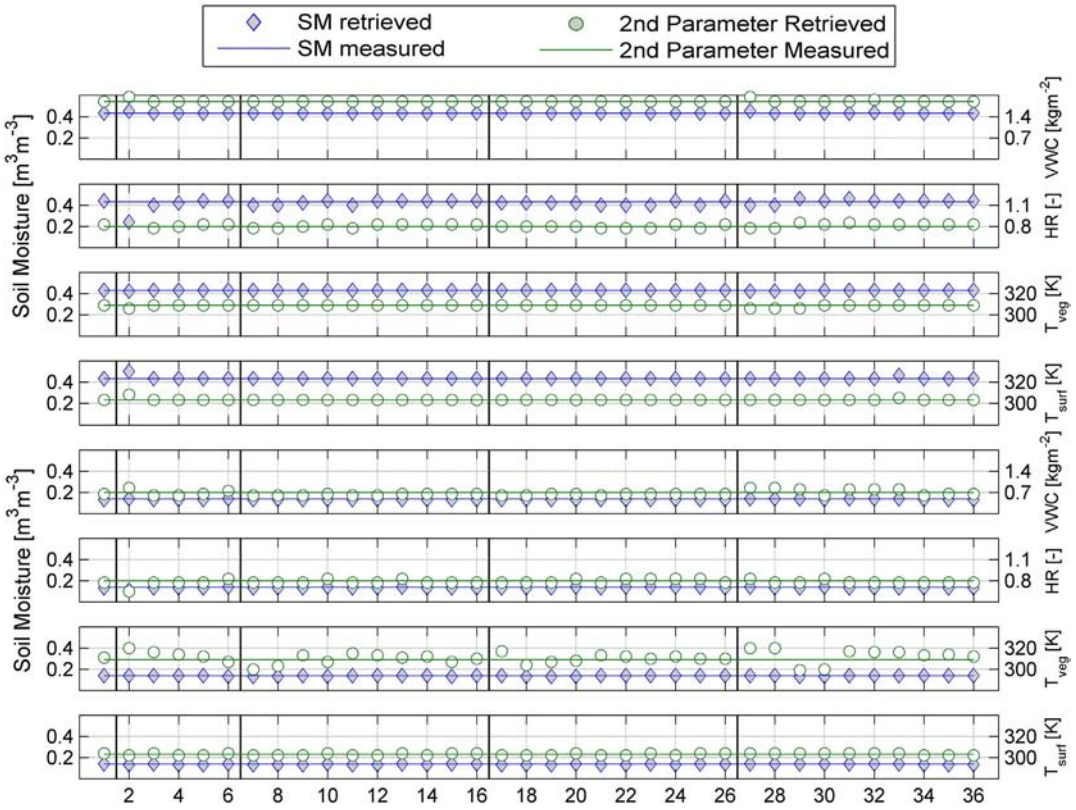

Fig. 5. Comparison of two-parameter retrieval results (blue diamond: SM, green circle: secondary parameter) against NAFE'05 ground measurements (blue line: measured SM; green line: second parameter ground truth) obtained from synthetic, dual-polarized TB data. Different angular group combinations (x-axis) were tested for the retrieval as given in Table 3. Note that in each plot the left y-axis corresponds to soil moisture and the right y-axis relates to the additionally retrieved parameter. The top four panels represent wet conditions and the bottom four panels illustrate dry conditions, respectively. (For interpretation of the references to color in this figure legend, the reader is referred to the web version of this article.)

was assumed that there were no NAFE'05 ground data available for these two parameters, and a feasible range of values was set for each individual parameter to simulate the multi-angular brightness temperature response. Table 2 presents the upper and lower limits used for each parameter. Consequently, soil moisture and one of either i) VWC, ii) H_R, iii) T_{veg}, or T_{surf} were varied – as opposed to the fixed parameter values used for TB_{ref} – to obtain the range of possible brightness temperature responses for each scenario pair.

Next, the root mean square error (RMSE) was calculated between the reference (TB_{ref}) and the simulated (TB_{sim}) brightness temperatures (see right side of Fig. 1), and the value stored in a RMSE matrix referring to the respective combination of parameter values of the scenario pair (see Table 2). This process was repeated numerous times – considering the varying amplitude in random TB error for the TB_{ref} simulation – until the difference between the RMSE matrix of the current iteration and the mean RMSE matrix calculated from the previous iterations was lower than a certain threshold. Hence, the final RMSE matrix illustrates a mean RMSE distribution map, describing the general sensitivity of the retrieval model, when 2 K > TB error > −2 K was considered. In order to examine the performance of multi-parameter retrievals from L-band data acquired at various incidence angles, the brightness temperature and RMSE model results were further classified into five angular groups of 0–10°, 10–20°, 20–30°, 30–40°, and 40–50°. Consequently, each of these five angular bins contained a minimum of ten TB measurements per polarization.

For validation of the results obtained from the simulated TB datasets, the airborne L-band observations from the NAFE'05 experiment were used. The airborne measurements were processed under the same angular configurations as the synthetic TB. The inverse L-MEB model retrieval results for SM, VWC, H_R, T_{veg} and T_{surf} were then compared to the NAFE'05 ground measurements and the possible angular preferences assessed.

4. Retrieval sensitivity to incidence angle configuration

With respect to the four available NAFE'05 campaign days, simulations were performed for all stages of soil moisture and vegetation water conditions. However, only the two moisture extremes, the very wet case with SM = 0.43 m^3 m^{-3}/VWC = 1.9 kg m^{-2}, and the dry case with SM = 0.14 m^3 m^{-3}/VWC = 0.7 kg m^{-2} are presented here, since the analysis of the remaining dates showed overall similar results.

4.1. Analysis of synthetic L-MEB simulated brightness temperatures

The iterative re-calculation of the mean RMSE between TB_{sim} and TB_{ref} yielded a mean RMSE distribution map for each two-parameter scenario that was tested (Fig. 2). The sensitivity of the retrieval model was assessed by initially focusing on the pattern of the RMSE evolution within the studied parameter space (SM and one additional parameter of VWC, H_R, T_{veg}, or T_{surf}), when all incidence angles and dual-polarized TB were considered. Across all four scenarios the derived RMSE contour lines indicated a single global minimum as depicted by Fig. 2. This implied that the minimization algorithm, which is the core process in the retrieval, will most likely approach the “true” solution rather than a local minimum. Moreover, the outline of the illustrated minimum can be used to interpret the precision of the retrieval within the considered two-parameter space. For example, a long valley may result in a large error due to random noise in the TB observations, which hampers the system to reach a definite solution. In particular, the retrieval scenarios SM–H_R and SM–T_{surf} demonstrated a long elliptical valley covering a wide range of H_R- and T_{surf}-values, respectively. The dominantly vertical extent of the minimum denotes low retrieval sensitivity to soil moisture and higher sensitivity to the parameter on the x-axis, which is simultaneously derived with soil moisture. The two remaining scenarios SM–T_{veg} and SM–VWC displayed better defined mean RMSE minima outlined by a more circular shape. Notably, the position and shape of the global minima shifted for all parameter combinations under dry conditions, generally leading to high retrieval sensitivity to soil moisture as well as to the additionally retrieved parameter. Note, the mean TB RMSE maps represent the general sensitivity of the retrieval model, and the effect of random TB uncertainty (in our case the impact of 2 K error in TB) is indicated by the standard deviation of the TB maps. We tested different options with TB errors of ±4 K and found that the shape of the global minima varied slightly but kept the general pattern of the mean TB pattern shown in Fig. 2. Thus, we concluded that the mean TB RMSE distribution is likely to be independent of the TB uncertainty that is chosen.

Subsequent separation of the mean dual-polarized TB RMSE pattern into five angular groups of 10° bins each is shown in Fig. 3. In general, better defined global minima of small circular extent were observed for large incidence angles, independent of the tested parameter space. Conversely, the mean TB RMSE pattern derived from an angular range of 0–10° demonstrated dominantly vertically or diagonally elongated minima. This behavior suggested a range of equi-possible parameter combinations of SM and the respective ancillary parameter, making it more difficult to find the correct solution. For dry conditions, the sensitivity to soil moisture increased slightly with respect to the more horizontally positioned minima in all angular cases and parameter combination.

Comparison of the two-parameter retrieval results with NAFE'05 ground measurements indicated no clear preference for any of the angular groups for both moisture states. All angular groups performed well for the soil moisture modeling. Though in the case of dry conditions, especially for the retrieval of the secondary parameter, there was a slight tendency towards less accurate parameter estimates from TB obtained at small to mid-range angles. This effect was rather distinct in the case of the SM–T_{veg} retrieval scenario.

Further analysis (not shown in this paper) of the retrieval model sensitivity, by separating the dual-polarized TB data into single-polarization, yielded a notably stronger scattering behavior of the retrieval results especially in the low- to mid-angular groups and for dry conditions — being most prominent for the T_{veg} retrieval. This implies that the vegetation structure and surface roughness effects on TB_H and TB_V differ substantially in those angular ranges and that the use of dual-polarization observations might smooth out the diverse contribution under such conditions. In contrast, TB_H and TB_V are almost equal when acquired at near-nadir views, so not much additional information is to be expected from dual-polarized TB.

4.2. Analysis of NAFE'05 airborne brightness temperatures

In terms of validating the synthetic study results, an additional analysis was carried out using the passive microwave measurements obtained during the NAFE'05 campaign. The data set was processed according to the same angular settings chosen for the synthetic model simulations, focusing on five angular groups of TB data. However, due to the PLMR configuration with its six fixed beams and slight variations in aircraft pitch across the sampling dates, not all angular groups were represented on all sampling days. An overview of results from the two-parameter retrievals per angular group, as compared with the NAFE'05 ground measurements, is presented in Fig. 4.

Contrary to the synthetic findings, the parameters were not accurately retrieved across all angular groups. Large deviations from the NAFE'05 ground measurements were observed for soil moisture and the simultaneously retrieved ancillary parameters. With the lower moisture conditions there was a slight improvement for the retrieved soil moisture in the SM–VWC and SM–T_{veg} scenarios, but the overall multi-angular model performance was still poor. Thus, two additional parameterizations were tested, which account differently for the non-nadir viewing impacts on the optical depth, through the vegetation structure parameters tt_H and tt_V (see Eq. (3)). The vegetation structure

plays an important role, especially for the wheat canopy of the NAFE'05 test site, as it is predominantly vertically structured in a mature state. As opposed to the initial configuration "P1" of $tt_H = 1$ and $tt_V = 8$ (Wigneron et al., 2007), alternate configurations "P2" with $tt_H = 0.2$ and $tt_V = 1.4$, both computed from the same experimental dataset in an earlier study (Peischl et al., 2012), and "P3" with $tt_H = 1$ and $tt_V = 1$ (referring to an isotropic case with no dependence on polarization and incidence angle) were also tested. The P3 parameterization is often used in the case of grass and pasture land cover types.

With respect to the mean TB RMSE pattern, similar results to P1 as illustrated in Figs. 2 and 3 were found, but with mostly elongated global minima, suggesting less retrieval sensitivity for P2 and P3. However, comparison of the P2 and P3 retrieved parameter estimates with the NAFE'05 measurements demonstrated a significant improvement for both the soil moisture as well as the secondary retrieved parameters. The retrieved soil moisture values were overall within the range of standard deviation except for a few cases, predominantly from the 10–20° angular group. Regarding the simultaneously retrieved ancillary parameter, satisfying results were observed for H_R and T_{surf}. In the case of the vegetation water content (VWC) as well as the vegetation temperature (T_{veg}), the model estimates were rather scattered with no specific trend for moist or dry conditions. In terms of an angular preference, results agreed with the synthetic findings from the dual-polarized retrieval, that there was no optimal result either when the soil was wet and the VWC high or when the soil moisture and the vegetation water content were low.

In summary out of the three model configurations studied, the initially tested parameterization P1 yielded unsatisfying results in contrary to its good performance in the synthetic analysis. Better retrieval estimates were obtained using the two alternate parameterizations, which considered either a minor or no angular dependence of the vegetation structure on the optical depth. Moreover, results from the airborne data suggested that a simultaneous retrieval of SM and H_R or T_{surf} was better posed than SM and either VWC or T_{veg}.

5. Cross-combination of multi-angular L-band data

Here the five previously assigned angular groups of synthetic TB data were merged into different combinations – mainly considering groups of opposite polarization – to investigate if particular combinations would lead to improved retrieval accuracy as opposed to focusing on a single-polarization and angular group. All tested cross-combinations are listed in Table 3 and the retrieval results are summarized in Fig. 5.

Qualitatively all retrieval results from the cross-combinations demonstrated mostly no or minor variations from the NAFE'05 ground measurements for soil moisture and its ancillary parameters. The particular angular groups which yielded peaks in the parameter estimations all had one aspect in common: that simulated TB data from small to mid-range angles (0–10° or 10–20°) was used for the retrieval. This feature was specifically prominent in the SM–T_{veg} scenario for the retrieval of T_{veg}, and a bit less pronounced for VWC or H_R estimates. A stepwise improvement of the modeled parameters was clearly related to the use of TB data from larger incidence angles in combination with the small angular TB data. Best results were obtained when the 0–10° observations were combined with the angles >40°, partially confirming the ground-based studies by Wigneron et al. (2004), who found that best soil moisture estimates were derived at H-polarization when the difference in angle was >30° for biangular measurements. Conversely, when V-polarized TB data from small angles was combined with large H-polarized TB data no significant improvement was observed.

The scattering behavior of the retrieval results regarding different angular cross-combinations was especially dominant under dry conditions (low soil moisture and vegetation water content). These effects are likely to be caused by the increased contribution of soil emission to the overall brightness temperature response. The reduced relative vegetation contribution to the overall brightness temperature response makes it more difficult to retrieve the desired vegetation properties. Moreover, the sensitivity to the effective surface soil roughness might change with moisture content since the soil emission originates from deeper layers of the soil column under dry conditions.

6. Conclusion

A two-step analysis of multi-parameter retrievals was conducted to investigate the sensitivity of the retrieval to the angular viewing configurations of an L-band radiometer. The analysis was based on synthetic and airborne multi-angle brightness temperature data acquired over a wheat canopy.

It was concluded from the angular synthetic data study that the circular global minima with small extent required for high retrieval sensitivity was generally achieved when dual-polarized brightness temperature measurements from large incidence angles (40–50°) were selected. The sensitivity of the retrieval model decreased when – in addition to the usage of TB data from small incidence angles – dry conditions in terms of low surface soil moisture and vegetation water content were observed. These circumstances also hampered the simultaneous retrieval of the ancillary data leading to stronger scattering of the model estimates across the tested angular groups. Combining microwave data acquired at different angles and polarization yielded the most significant retrieval enhancements, where TB data obtained jointly at angles between 0 and 10° (H-polarized) and 40–50° (V-polarized) were used.

The validation study confirmed the synthetic results in terms of a preference for dual-polarized over single-polarized microwave data for two-parameter retrievals. However, best retrieval results were often derived when the characterization of the vegetation structure parameters was adjusted from $tt_H = 1$, $tt_V = 8$ to $tt_H = 0.2$, $tt_V = 1.4$ (calibrated values for wheat) or even $tt_H = 1$, $tt_V = 1$ (implying little/no angular/polarization dependency). However, these parameter values also yielded more elongated global minima, suggesting lower retrieval accuracy. Moreover, the airborne retrieval did not confirm the synthetic findings based on the extent of the global minima that retrievals at small angles were generally less accurate than other angular groups.

Overall, both the synthetic and the airborne results showed that a simultaneous retrieval of SM–VWC or SM–T_{veg} was less preferable to SM–HR or SM–T_{surf} retrievals, based on the highly variable results that were obtained. Especially in the case of dry conditions when the relative vegetation contribution to the composite TB signal is decreasing, it was complicated to retrieve information about the canopy independent of the vegetation structure parameterization we applied.

Acknowledgment

The authors would like to acknowledge the National Airborne Field Experiment 2005 team for collecting and providing the data set used in this study. The NAFE'05 campaign has been made possible through infrastructure (LE0453434 and LE0560930) and research (DP0557543 and DP0556941) funding from the Australian Research Council. This study was financially supported by Australian Research Council grant DP0879212 in the framework of the MoistureMap project. The authors appreciate the helpful feedback by the reviewers which improved the manuscript substantially.

References

Calvet, J. -C., Wigneron, J. -P., Walker, J. P., Karbou, F., Chanzy, A., & Albergel, C. (2011). Sensitivity of passive microwave observations to soil moisture and vegetation water content: L-band to W-band. *IEEE Transactions on Geoscience and Remote Sensing, 49*(4), 1190–1199, http://dx.doi.org/10.1109/TGRS.2010.2050488.

Camps, A. J., Gourrion, J., Tarongi, J. M., Gutierrez, A., Barbosa, J., & Castro, R. (2010, 25–30 July). RFI analysis in SMOS imagery. *Paper presented at the IEEE International Geoscience and Remote Sensing Symposium (IGARSS), Honolulu, Hawaii, USA, 2007–2010*, http://dx.doi.org/10.1109/IGARSS.2010.5654268.

Castro, R., Gutierrez, A., & Barbosa, J. (2012). A first set of techniques to detect radio frequency interferences and mitigate their impact on SMOS data. *IEEE Transactions on Geoscience and Remote Sensing*, *50*(5), 1440–1447, http://dx.doi.org/10.1109/tgrs.2011.2179304.

de Rosnay, P., Calvet, J. -C., Kerr, Y., Wigneron, J. -P., Lemaître, F., Escorihuela, M. J., et al. (2006). SMOSREX: A long term field campaign experiment for soil moisture and land surface processes remote sensing. *Remote Sensing of Environment*, *102*(3–4), 377–389, http://dx.doi.org/10.1016/j.rse.2006.02.021.

Dobson, M. C., Ulaby, F. T., Hallikainen, M. T., & El-Rayes, M.A. (1985). Microwave dielectric behavior of wet soil—Part II: Dielectric mixing models. *IEEE Transactions on Geoscience and Remote Sensing*, *GE-23*(1), 35–46, http://dx.doi.org/10.1109/TGRS.1985.289498.

Jackson, T. J. (1993). III. Measuring surface soil moisture using passive microwave remote sensing. *Hydrological Processes*, *7*(2), 139–152, http://dx.doi.org/10.1002/hyp.3360070205.

Jackson, T. J., Le Vine, D.M., Hsu, A. Y., Oldak, A., Starks, P. J., Swift, C. T., et al. (1999). Soil moisture mapping at regional scales using microwave radiometry: The Southern Great Plains hydrology experiment. *IEEE Transactions on Geoscience and Remote Sensing*, *37*(5), 2136–2151, http://dx.doi.org/10.1109/36.789610.

Jackson, T. J., & Schmugge, T. J. (1991). Vegetation effects on the microwave emission of soils. *Remote Sensing of Environment*, *36*(3), 203–212, http://dx.doi.org/10.1016/0034-4257(91)90057-D.

Kerr, Y. H., Font, J., Waldteufel, P., & Berger, M. (2000). The Soil Moisture and Ocean Salinity Mission—SMOS. *ESA Earth Observation Quarterly*(66), 18–26.

Kerr, Y. H., Waldteufel, P., Richaume, P., Wigneron, J. -P., Ferrazzoli, P., & Gurney, R. J. (2011). SMOS level 2 processor for soil moisture — Algorithm Theoretical Based Document (ATBD). *Report. CBSA, SO-TN-ESL-SM-GS-0001. Issue 3.e, CESBIO, Toulouse, France, 24.01.2011*.

Kerr, Y. H., Waldteufel, P., Richaume, P., Wigneron, J. -P., Ferrazzoli, P., Mahmoodi, A., et al. (2012). The SMOS soil moisture retrieval algorithm. *IEEE Transactions on Geoscience and Remote Sensing*, *50*(5), 1384–1403, http://dx.doi.org/10.1109/tgrs.2012.2184548.

Kerr, Y. H., Waldteufel, P., Wigneron, J. -P., Delwart, S., Cabot, F., Boutin, J., et al. (2010). The SMOS mission: New tool for monitoring key elements of the global water cycle. *Proceedings of the IEEE*, *98*(5), 666–687, http://dx.doi.org/10.1109/JPROC.2010.2043032.

Kerr, Y. H., Waldteufel, P., Wigneron, J. -P., Martinuzzi, J. M., Font, J., & Berger, M. (2001). Soil moisture retrieval from space: The Soil Moisture and Ocean Salinity (SMOS) mission. *IEEE Transactions on Geoscience and Remote Sensing*, *39*(8), 1729–1735, http://dx.doi.org/10.1109/36.942551.

McMullan, K. D., Brown, M.A., Martin-Neira, M., Rits, W., Ekholm, S., Marti, J., et al. (2008). SMOS: The payload. *IEEE Transactions on Geoscience and Remote Sensing*, *46*(3), 594–605, http://dx.doi.org/10.1109/Tgrs.2007.914809.

Merlin, O., Walker, J. P., Panciera, R., Young, R., Kalma, J., & Kim, E. J. (2007, December). Soil moisture measurement in heterogeneous terrain. *Paper presented at the 17th International Congress on Modelling and Simulation (MODSIM), New Zealand* (pp. 2604–2610).

Mo, T., Choudhury, B. J., Schmugge, T. J., Wang, J. R., & Jackson, T. (1982). A model for microwave emission from vegetation-covered fields. *Journal of Geophysical Research*, *87*(C13), 11,229–211,237, http://dx.doi.org/10.1029/JC087iC13p11229.

Njoku, E. G., & Entekhabi, D. (1996). Passive microwave remote sensing of soil moisture. *Journal of Hydrology*, *184*(1–2), 101–129, http://dx.doi.org/10.1016/0022-1694(95)02970-2.

Oliva, R., Daganzo-Eusebio, E., Kerr, Y. H., Mecklenburg, S., Nieto, S., Richaume, P., et al. (2012). SMOS radio frequency interference scenario: Status and actions taken to improve the RFI environment in the 1400–1427-MHz passive band. *IEEE Transactions on Geoscience and Remote Sensing*, *50*(5), 1427–1439.

Panciera, R., Allahmoradi, M., Merlin, O., Young, R., & Walker, J. P. (2009, November). *The Hydraprobe Data Acquisition System (HDAS) V.5: User guide. [V.1 created: September 2006]*. Australia: University of Melbourne, Melbourne (5).

Panciera, R., Walker, J. P., Kalma, J.D., Kim, E. J., Hacker, J., Merlin, O., et al. (2008). The NAFE'05/CoSMOS data set: Toward SMOS soil moisture retrieval, downscaling, and assimilation. *IEEE Transactions on Geoscience and Remote Sensing*, *46*(3), 736–745, http://dx.doi.org/10.1109/Tgrs.2007.915403.

Peischl, S., Walker, J. P., Ryu, D., Kerr, Y. H., Panciera, R., & Rüdiger, C. (2012). Wheat canopy structure and surface roughness effects on multiangle observations at L-band. *IEEE Transactions on Geoscience and Remote Sensing*, *50*(5), 1498–1506, http://dx.doi.org/10.1109/tgrs.2011.2174644.

Saleh, K., Wigneron, J. -P., Calvet, J. -C., Lopez-Baeza, E., Ferrazzoli, P., Berger, M., et al. (2004). The EuroSTARRS airborne campaign in support of the SMOS mission: First results over land surfaces. *International Journal of Remote Sensing*, *25*(1), 177–194, http://dx.doi.org/10.1080/0143116031000116444.

Schmugge, T. J., Jackson, T., Kustas, W. P., & Wang, J. R. (1992). Passive microwave remote sensing of soil moisture: Results from HAPEX, FIFE and MONSOON 90. *ISPRS Journal of Photogrammetry and Remote Sensing*, *47*(2–3), 127–143, http://dx.doi.org/10.1016/0924-2716(92)90029-9.

Schmugge, T. J., O'Neill, P., & Wang, J. R. (1986). Passive microwave soil moisture research. *IEEE Transactions on Geoscience and Remote Sensing*, *GE-24*(1), 12–22, http://dx.doi.org/10.1109/TGRS.1986.289584.

Schmugge, T. J., Wang, J. R., & Asrar, G. (1988). Results from the push broom microwave radiometer flights over the Konza Prairie in 1985. *IEEE Transactions on Geoscience and Remote Sensing*, *26*(5), 590–596.

Walker, J. P., & Houser, P. R. (2004). Requirements of a global near-surface soil moisture satellite mission: Accuracy, repeat time, and spatial resolution. *Advances in Water Resources*, *27*(8), 785–801, http://dx.doi.org/10.1016/j.advwatres.2004.05.006.

Wigneron, J. -P., Calvet, J. -C., de Rosnay, P., Kerr, Y. H., Saleh, K., Escorihuela, M. J., et al. (2004). Soil moisture retrievals from biangular L-band passive microwave observations. [Abstract]. *IEEE Geoscience and Remote Sensing Letters*, *1*(4), 277–281, http://dx.doi.org/10.1109/LGRS.2004.834594.

Wigneron, J. -P., Calvet, J. -C., Kerr, Y. H., Chanzy, A., & Lopes, A. (1993). Microwave emission of vegetation: Sensitivity to leaf characteristics. *IEEE Transactions on Geoscience and Remote Sensing*, *31*(3), 716–726, http://dx.doi.org/10.1109/36.225537.

Wigneron, J. -P., Calvet, J. -C., Pellarin, T., Van de Griend, A. A., Berger, M., & Ferrazzoli, P. (2003). Retrieving near-surface soil moisture from microwave radiometric observations: Current status and future plans. *Remote Sensing of Environment*, *85*(4), 489–506, http://dx.doi.org/10.1016/S0034-4257(03)00051-8.

Wigneron, J. -P., Kerr, Y. H., Chanzy, A., & Jin, Y. -Q. (1993). Inversion of surface parameters from passive microwave measurements over a soybean field. *Remote Sensing of Environment*, *46*(1), 61–72, http://dx.doi.org/10.1016/0034-4257(93)90032-S.

Wigneron, J. -P., Kerr, Y. H., Waldteufel, P., Saleh, K., Escorihuela, M. J., Richaume, P., et al. (2007). L-band Microwave Emission of the Biosphere (L-MEB) model: Description and calibration against experimental data sets over crop fields. *Remote Sensing of Environment*, *107*(4), 639–655, http://dx.doi.org/10.1016/j.rse.2006.10.014.

Wigneron, J. -P., Schmugge, T. J., Chanzy, A., Calvet, J. -C., & Kerr, Y. H. (1998). Use of passive microwave remote sensing to monitor soil moisture. *Agronomie*, *18*(1), 27–43, http://dx.doi.org/10.1051/agro:19980102.

Wigneron, J. -P., Waldteufel, P., Chanzy, A., Calvet, J. -C., & Kerr, Y. H. (2000). Two-dimensional microwave interferometer retrieval capabilities over land surfaces (SMOS Mission). *Remote Sensing of Environment*, *73*(3), 270–282, http://dx.doi.org/10.1016/S0034-4257(00)00103-6.